

ObjFiller-3D: Consistent Multi-view 3D Inpainting via Video Diffusion Models

Haitang Feng¹ Jie Liu^{1, ✉} Jie Tang¹ Gangshan Wu¹

Beiqi Chen³ Jianhuang Lai⁴ Guangcong Wang^{2, ✉}

¹Nanjing University ²Great Bay University

³Harbin Institute of Technology ⁴Sun Yat-sen University

Project page: <https://objfiller3d.github.io>

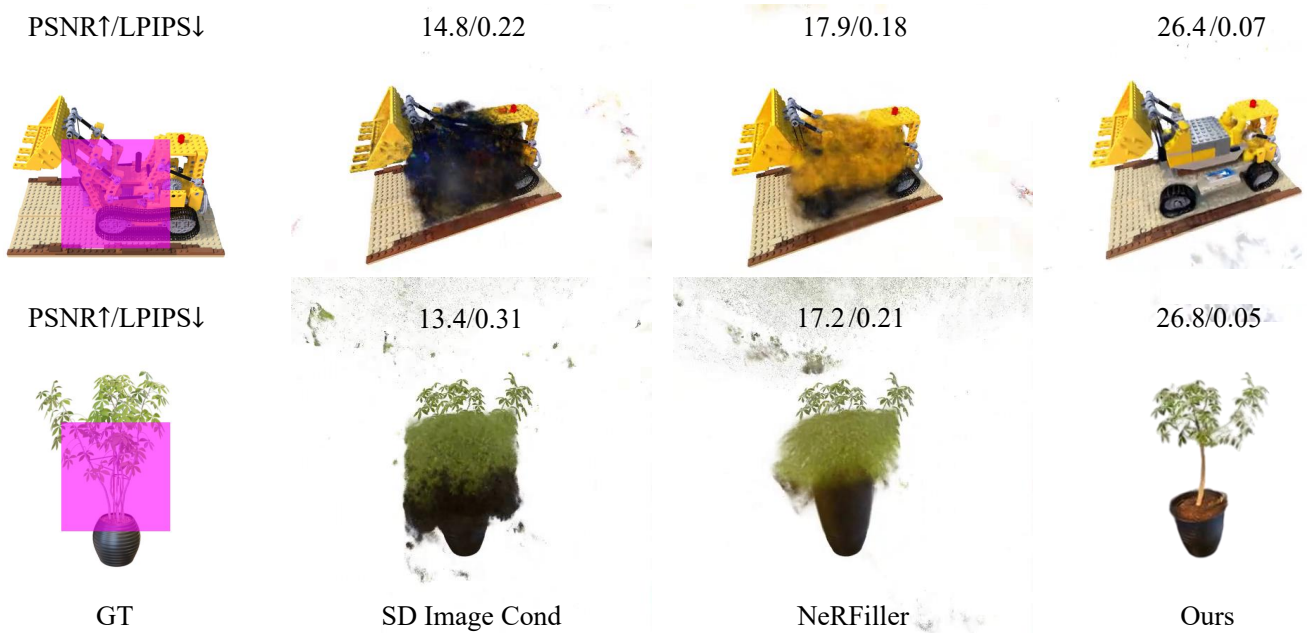


Figure 1. We introduce ObjFiller-3D, a novel framework capable of reconstructing complete 3D objects from partial inputs. Regions requiring inpainting are explicitly marked in pink. ObjFiller-3D demonstrates superior performance compared to previous state-of-the-art (SOTA) methods across multiple benchmark datasets.

Abstract

3D inpainting often relies on multi-view 2D image inpainting, where the inherent inconsistencies across different inpainted views can result in blurred textures, spatial discontinuities, and distracting visual artifacts. These inconsistencies pose significant challenges when striving for accurate and realistic 3D object completion, particularly in applications that demand high fidelity and structural coherence. To overcome these limitations, we propose ObjFiller-3D, a novel method designed for the completion and edit-

ing of high-quality and consistent 3D objects. Instead of employing a conventional 2D image inpainting model, our approach leverages a curated selection of state-of-the-art video editing model to fill in the masked regions of 3D objects. We analyze the representation gap between 3D and videos, and propose an adaptation of a video inpainting model for 3D scene inpainting. In addition, we introduce a reference-based 3D inpainting method to further enhance the quality of reconstruction. Experiments across diverse datasets show that compared to previous methods, ObjFiller-3D produces more faithful and fine-grained reconstructions (PSNR of 26.6 vs. NeRFiller (15.9) and LPIPS of 0.19 vs. Instant3dit (0.25)). Moreover, it demon-

✉: Jie Liu and Guangcong Wang are co-corresponding authors.
Email: liujie@nju.edu.cn, wanggc3@gmail.com

strates strong potential for practical deployment in real-world 3D editing applications.

1. Introduction

Repairing incomplete 3D objects is a crucial task in computer graphics and computer vision, particularly in applications such as cultural heritage restoration and digital reconstruction. Environmental constraints during scanning often result in data loss, which poses significant challenges in recovering the original geometry of objects. Despite its importance, research on 3D object completion remains relatively scarce—to the best of our knowledge, only methods such as NeRFiller [49] and Instant3dit [2] focused on this problem—and the task is fundamentally distinct from 3D generation and mainstream editing tasks.

3D generation methods [23, 52] typically aim to produce high-quality 3D assets from noise, a single image, or a few reference views. These approaches generally assume that the input images depict complete views of the object and are not designed to handle partial or degraded observations. On the other hand, mainstream 3D editing [10] focuses on modifying textures or performing style transfer, without accommodating significant geometric alterations, which making it unsuitable for restoring missing object parts.

One straightforward approach is to use a 2D inpainting model [27, 41] to restore multiple view images of the incomplete object, and then apply a pre-trained 3D generation model to synthesize the full 3D object. A key challenge is that conventional 2D inpainting does not account for cross-view dependencies of the same object, often resulting in inconsistent outputs across different views (see Figure 5). Using these mismatched images for reconstruction inevitably leads to artifacts and poor quality results. Score-Distillation Sampling (SDS) [32] and Iterative Dataset Update (IDU) [10] have been proposed to address this challenge. However, both SDS and IDU rely on the iterative optimization of 3D models from numerous inconsistent 2D samples. As a result, the optimization process is extremely time-consuming and often leads to blurry or inaccurate reconstructions. Moreover, they do not support local high-quality 3D editing.

Recent studies NeRFiller [49] and Instant3dit [2] focused on 3D Object inpainting based on state-of-the-art (SOTA) 3D representations. NeRFiller observes that denoising four missing view images arranged in a 2x2 grid leads to more consistent multi-view inpainting compared to independent inpainting, referring to this as a grid prior. Instant3dit builds upon the grid prior of NeRFiller. They introduced a masked object dataset, and trained a Stable Diffusion inpainting model [27], specifically designed to generate consistent 2x2 grid images. The inpainted multi-view images are then used as input for the Large Recon-

struction Model (LRM) [14] to quickly produce the full 3D reconstruction. Although these approaches have attempted to address 3D inpainting based on SOTA 3D representations, the primary limitation is that they ensure consistency across only four views, thereby restricting the number of supported viewpoints, and thus leading to lack of details in geometry and textures. They are only suitable for objects with simple structure and uniform textures. They struggle with challenging tasks involving complex shapes and many views, failing to guarantee high-quality reconstructions. On the other hand, the current cutting-edge video generation [13, 43, 56], video editing [18, 45], and world models [9] have showcased the strong spatial perception and understanding capabilities of video models. These models excel in maintaining inter-frame consistency, enabling the generation of 3D-consistent and coherent objects. Previous works [42] have already explored using video models for 3D generation tasks but did not consider 3D object inpainting.

Motivated by the limitation of the existing 3D inpainting models and the advantages of video generation methods, we analyze the representation gap between 3D and videos. We observe that 3D scenes are typically modeled with 360-degree coverage and uniform spatial sampling, enabling complete view synthesis, whereas real-world videos are limited to partial viewpoints, dynamic content, and non-uniform temporal sampling (e.g., slow-fast encoding), which introduce challenges like deformation, occlusion, and motion blur—less prominent in static 3D settings. We adapt the video inpainting model to a 3D inpainting model with Low-Rank Adaptation (LoRA) [15]. To guarantee the 360-degree looped video inpainting, we also duplicate the first image frame as the last one. To support reference-driven 3D inpainting, We prepend the reference image and an all-zero mask to the video and mask sequences, respectively, indicating no editing is required for the first frame.

The results demonstrate that our method clearly outperforms prior approaches in quality while maintaining a short runtime, achieving SOTA performance. Specifically, ObjFiller-3D achieves more faithful and fine-grained 3D reconstructions, outperforming NeRFiller and Instant3dit with a PSNR of 26.6 (vs. 15.9) and an LPIPS of 0.19 (vs. 0.25), respectively.

To summarize, our main contributions include: 1) We propose a highly consistent 3D object inpainting method that generates high-quality results within a short time, surpassing previous methods and not being limited by the number of viewpoints. 2) We present a new video-to-3D adaptation method that supports high-quality 3D inpainting by efficiently leveraging pre-trained video editing models. Moreover, we introduce a reference-based 3D inpainting to enable image-based conditional generation. 3) Extensive experiments validate the effectiveness of our method and highlight its substantial improvement over prior ap-

proaches.

2. Related Work

Our objective is to complete the missing regions of an existing 3D object. Several approaches are relative this problem, including 3D object generation and editing as well as video inpainting.

2.1. 3D Object Generation

3D object generation methods are typically categorized into 2D prior-based and feedforward approaches. The former utilizes image generative models (e.g., Stable Diffusion [34], Imagen [35]) trained on large-scale datasets like LAION-400M/5B [36, 37] to extend text or image inputs into 3D. DreamFusion [32] introduced Score Distillation Sampling (SDS) for this purpose, followed by improved but costly variants [16, 48]. Alternatively, some methods [8, 17, 24, 26, 38, 39, 44] directly generate multi-view consistent images using finetuned diffusion models, offering a more efficient path to 3D reconstruction. Feedforward generation is another key paradigm for 3D synthesis, often employing encoder-decoder architectures like Latent Diffusion Models (LDMs) [34] to extract image tokens and generate latent 3D representations. Models such as Large Reconstruction Model (LRM) [14], MeshLRM [50], Instant3D [23], and InstantMesh [53] use Transformers to map tokens into implicit triplane representations.

2.2. 3D Editing

Recent advances in 3D field editing mainly leverage NeRF [29] and 3DGS [20] for superior realism and flexibility over traditional mesh or point clouds. Instruction-guided methods use pre-trained 2D diffusion models due to scarce 3D data, optimizing NeRF via Score Distillation Sampling (SDS) to achieve view-consistent, relightable 3D outputs. Iterative Dataset Update (IDU) approaches like Instruct-NeRF2NeRF [10] train 3D scenes using edited images. Methods [4, 5, 47] extend 3DGS for efficient, controllable editing. For 3D object removal, SPIn-NeRF [30] combines depth and 2D inpainting but struggles with full 360° views. Recent Gaussian Splatting inpainting works like InFusion [25], AuraFusion360 [51], and IMFine [40] address 360° unbounded scene restoration. However, these methods primarily concentrate on maintaining global scene consistency and eliminating visual artifacts after object removal, which differs substantially from the goals of our task.

Among the most closely related methods to ours are NeRFiller [49] and Instant3dit [2]. However, NeRFiller still relies on IDU, and Instant3dit is limited to handling only four input views, which constraints their performance.

2.3. Video Inpainting

Unlike image inpainting, video inpainting requires consistency across frames, which makes the task more challenging. Methods [7, 54, 59] utilize flow-guided feature propagation in conjunction with video Transformer architectures to reconstruct missing content across frames. The emergence of video foundation models [3, 21, 43] in recent research has demonstrated remarkable competitiveness. Building upon the video generation model WAN [43], VACE [18] demonstrates strong capabilities in the domain of video editing and inpainting. However, these models are trained on real-world, scene-level video datasets [46, 55], which differ fundamentally from object-centric 3D model datasets [6]. The complex, multi-object environments in real-world data introduce inductive biases that challenge direct transfer. Therefore, effective application of such video models to 3D-specific tasks necessitates domain adaptation to mitigate the domain discrepancy.

3. Method

We present ObjFiller-3D, a new framework that involves controllable modifications of the geometry, appearance, or semantics of 3D scenes or objects. In the following, we detail the process of obtaining 3D-consistent masks, organizing existing datasets [2] for finetuning the VACE model [18], and generating the final 3D object.

3.1. Preliminary and Problem Formulation

Preliminary. 3D Gaussian Splatting (3DGS) [20] uses 3D Gaussians as scene primitives and represents the scene with a large number of 3D Gaussians. A Gaussian ellipsoid centered at point $\mu \in \mathbb{R}^3$ (mean) with covariance matrix Σ can be written as:

$$G(x) = e^{-\frac{1}{2}x^T \Sigma^{-1}x}, \quad \text{and} \quad \Sigma = RSS^T R^T, \quad (1)$$

where x denotes the distance from a specific point in space to the mean μ , and $R \in \mathbb{R}^{3 \times 3}$ represents the Gaussian’s rotation matrix, while $S \in \mathbb{R}^{3 \times 3}$ represents the scaling matrix. After formalizing the 3D Gaussians, volumetric rendering techniques [19] can be used to “splat” these Gaussians onto the 2D image plane. Specifically, the color c for a pixel along a ray is given by:

$$c = \sum_i c_i \alpha_i G(x_i) \prod_{j=1}^{i-1} (1 - \alpha_j G(x_j)), \quad (2)$$

where $\alpha \in \mathbb{R}$ and $c \in \mathbb{R}^3$ represent the opacity and color of the 3D Gaussians, respectively. 3DGS is recognized for its efficiency in real-time radiance field rendering and has thus been integrated into our method.

Problem Formulation. We define the task of 3D object inpainting as follows: Given an incomplete 3D object O , a

3D mask region M , a text description y of the object and an optional reference image I_r , our goal is to generate a plausible shape O' contained within M , based on y and I_r , such that $\{O \cup O'\}$ forms a complete 3D object.

3.2. Dataset Preparation

Before introducing our proposed method, we first describe the dataset used in Instant3dit. Specifically, Instant3dit utilizes approximately 7k high-quality 3D objects selected from the large-scale synthetic dataset Objaverse [6]. Furthermore, it defines three distinct types of 3D masks, namely: convexhull, surface, and volume (see Figure 2). 1) *Convexhull*: the inpainted part of the object O' is fully contained inside the mask M . 2) *Surface*: the mask M covers a small surface region on object O . 3) *Volume*: the mask M tightly encloses the object O .



Figure 2. Three Types of 3D Masks.

Although the Instant3dit dataset provides masked objects along with their corresponding 3D masks, it does not include the original complete objects or their associated 2D ground truth images. To address this, we locate the corresponding objects from the Objaverse dataset for each object in Instant3dit, and render 16-view 2D images at a resolution of 512×512 using Blender as ground truth. These 16 views are distributed at a fixed elevation of 20 degrees, with azimuth angles uniformly sampled from 0 to 2π .

Additionally, we employ Cap3D [28] to produce captions for individual 3D objects, which use the pre-trained model in captioning (BLIP-2 [22]), alignment (CLIP [33]), and LLM (GPT4 [1]) to consolidate multi-view information.

To leverage the inpainting prior from a generative video diffusion model, we need to project the 3D information onto 2D plane. We render each 3D object O into a set of image frames $F_s = \{f_1, f_2, \dots, f_n\}$, and the missing region M into a set of binary masks $M_s = \{m_1, m_2, \dots, m_n\}$, from our predefined camera poses $\Pi = \{\pi_i\}_{i=1}^n$.

$$\langle f_i, m_i \rangle = \mathcal{R}(O, M, \pi_i), \quad i \in \{1, \dots, n\}. \quad (3)$$

\mathcal{R} denotes a rendering operator. The complete dataset is approximately 18 GB in size, and we will make it publicly available upon publication.

3.3. Multi-view Consistent 3D Inpainting

We leverage the inter-frame coherence of video models to maintain consistent 3D inpainting across multiple views. Specifically, after processing the Instant3dit dataset, each object is represented as a tuple $\langle F_s, M_s, y \rangle$, where the 16 rendered views form a 360° looped video. To meet VACE’s [18] input requirement of $4n + 1$ frames, we duplicate the first image and mask as the 17th frame. The image frames F_s and masks M_s are combined into video sequences, which—along with y and I_r —are fed into the VACE model to generate F'_s , a set of temporally consistent and inpainted frames.

Analyzing Representation Gap between 3D and Videos.

While video-based editing methods offer temporal context, they often struggle to capture the full spatial structure and semantic consistency required in 3D content creation. First, 3D scenes and objects are generally modeled with 360-degree coverage, yielding looped rendered videos, while real-world videos are inherently limited to partial and forward-facing views. Second, real-world videos frequently contain dynamic objects and temporal motions, which introduce complexities such as object deformation, occlusion, and motion blur—issues that are less prevalent in static 3D editing scenarios. Third, videos are typically encoded using non-uniform temporal sampling schemes, such as slow-fast strategies that emphasize specific motion segments, whereas 3D data is often uniformly sampled in space for structural completeness. Serving as a counterexample, the LoRA ablation in the subsequent experimental section showcases results obtained using the video model without any alterations.

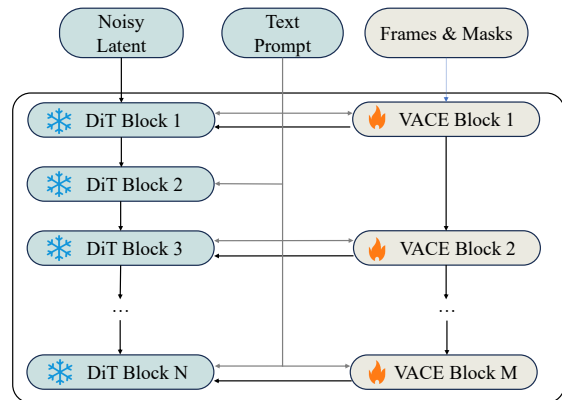


Figure 3. **VACE model architecture.** VACE blocks control the output of the WAN model through adapter tuning, based on control signals such as text prompts and masks, enabling controllable video editing. We inject LoRA into the VACE layers and freeze all other parameters.

Adapting Video Inpainting to 3D Inpainting. To bridge the gap between video inpainting and 3D inpainting, we

finetune the video diffusion model with Low-Rank Adaptation [15] method. Figure 3 illustrates the main architecture of the VACE model, where LoRA weights are incorporated into every VACE transformer layer. During training, the original parameters of the transformer blocks are kept frozen, and only the low-rank matrices $A \in \mathbb{R}^{d \times r}$ and $B \in \mathbb{R}^{r \times k}$ are updated, with the rank $r \ll \min(d, k)$. We set LoRA rank $r = 32$.

To train the video inpainting model parameter θ , we adopt the flow matching loss that aligns the learned velocity field with the ground-truth flow. Let $u_\theta(t, x | F_s, M_s, y)$ denote the velocity predicted by our diffusion network at time t and state x . Let $u^*(t, x)$ be the true velocity field defined by the underlying interpolation between noise and data distributions. The flow matching loss is then defined as

$$\mathcal{L}_{\text{FM}}(\theta) = \mathbb{E}_{t \sim \mathcal{U}(0,1)} \mathbb{E}_{x \sim p_t} \left\| u_\theta(t, x | F_s, M_s, y) - u^*(t, x) \right\|_2^2, \quad (4)$$

where p_t denotes the marginal distribution of the noisy data at time t , and $\mathcal{U}(0, 1)$ denotes the uniform distribution over the interval $[0, 1]$. Minimizing \mathcal{L}_{FM} encourages the network to recover the true continuous flow from noise to data, yielding temporally coherent inpainted frames.

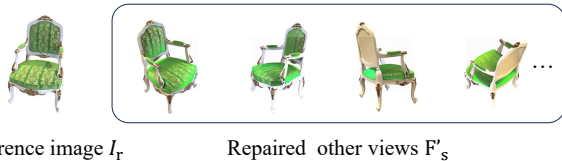


Figure 4. **Reference-based 3D Inpainting.** Given a reference image, the other views are well aligned with the input.

Reference-based 3D Inpainting. Without reference images, inpainting results often vary widely and may require multiple generations to achieve a desirable outcome. However, in certain scenarios—such as restoring historical architecture or cultural artifacts—we typically have access to a complete reference image to guide the inpainting process and ensure results align with expectations. This is straightforward for our method, as the VACE model has designed to handle video editing based on reference images. Specifically, we can append the reference image I_r to the input video sequence F_s as the first frame. Correspondingly, we include an all-zero mask as the first frame in the mask sequence M_s , indicating that this frame does not require editing. After generating the video, this auxiliary frame can be discarded. Figure 4 presents an inpainting result with a reference image.

Object Reconstruction. After the inpainting process, we obtain a set of frames F'_s along with their corresponding camera poses Π . These inpainted views can then be used

to reconstruct the complete 3D object represented by a 3D Gaussians \mathcal{G} .

$$\mathcal{G}_{\text{inpainted}} = \arg \min_{\mathcal{G}} \sum_{\pi_i \in \Pi, f'_i \in F'_s} \mathcal{L}(\mathcal{R}(\mathcal{G}, \pi_i), f'_i), \quad (5)$$

where \mathcal{R} represents the rendering function, while \mathcal{L} is 3DGS’s loss function. This reconstruction approach is similar to the NeRFiller pipeline, but thanks to the high consistency ensured during our inpainting step, we are able to skip the IDU stage. This significantly reduces reconstruction time: our method completes the process in under 10 minutes, whereas NeRFiller [49] requires over 40 minutes. Moreover, our reconstruction quality substantially surpasses that of NeRFiller, as shown in Figure 1 and Figure 5.

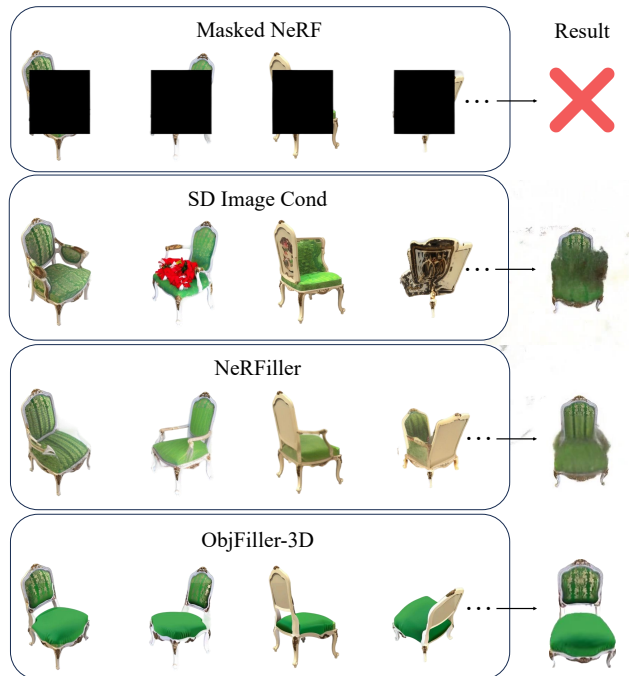


Figure 5. **Visual comparison of different multi-view inpainting methods** Compared to baseline approaches, ObjFiller-3D achieves more consistent and coherent inpainting across different views.

4. Experiments

Implementation details. We train our models using 3,000 objects from our reprocessed dataset. During the training phase, we set the LoRA rank to 32, used a learning rate of 10^{-4} , a batch size of 4, and trained for 10 epochs. For the VACE 14B model, training was conducted in half-precision, consuming approximately 60 GB of VRAM. The process took approximately 3 days on a single NVIDIA A800 GPU. During inference, we used the UniPC sampler [58], with the

number of inference steps set to 20, a CFG [12] guidance scale of 4, and a LoRA scale of 1.

Evaluation Metrics. For the metric comparison between ours and Instant3dit, we focus on three key aspects: 1) *Text-Image Similarity*: We measure the semantic relevance between the generated 2x2 grid images and the given text prompt using the CLIP [33] similarity score. 2) *Image Quality and Fidelity*: This evaluates the quality of the generated images and the similarity between the inpainted images and the Ground-Truth (GT) images. Specifically, we inpaint 300 grid images from the evaluation dataset and compare them against GT grids using the FID score [11]. 3) *multi-view Consistency*: To assess consistency across the four views in the inpainted grid image, we feed the four images directly into LRM [53]. If the views lack consistency, LRM will produce a distorted object; otherwise, the reconstruction will be coherent. To quantify this, we render the resulting object from the original viewpoints and compute the perceptual LPIPS score [57] between the rendered images and the inpainted ones. A lower LPIPS score indicates better multi-view consistency. For the metric comparison between ours and NeRFfiller, the final object reconstruction is a 3D reconstruction task. Therefore, we evaluate using three standard metrics: SSIM, PSNR, and LPIPS.

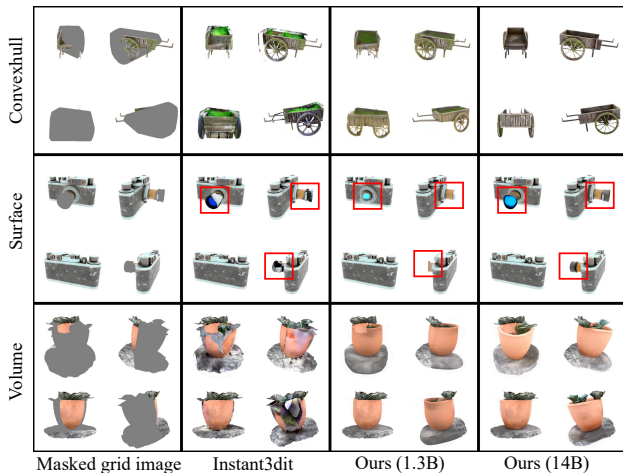


Figure 6. **Qualitative results compare to Instant3dit** We apply our method to three different mask types, listed from top to bottom as Convexhull, Surface, Volume. ObjFiller-3D-14B (the rightmost column) exhibits the highest consistency across all the mask types.

4.1. Comparisons with State-of-the-Arts

Comparison with Instant3dit. We provide four model variants: VACE1.3B, VACE14B, and their respective LoRA fine-tuned versions. We evaluate them on 300 held-out objects. For Instant3dit, we stack masked multi-view images and corresponding masks from four orthogonal viewpoints (0° , 90° , 180° , and 270°) into 300 image grids arranged in a

2x2 layout. These image grids, along with text prompts generated by Cap3D [28], serve as input to Instant3dit’s open-source 2D multi-view inpainting model, which has been trained on SDXL [31]—exactly as expected by its design. For the four VACE variants, we respectively concatenate all views and masks into 17-frame videos, and feed them into VACE along with text prompts. From the output video, we extract the same four orthogonal views and arrange them into 2x2 image grids. Since object reconstruction in later steps is performed using LRM for all methods, our comparison focuses solely on the visual quality of the image grids generated by VACEs and Instant3dit.

Comparison with NeRFfiller. We choose VACE14B-LoRA followed with 3DGS as our main model for comparison with NeRFfiller. For a more comprehensive evaluation, we additionally consider two alternative methods: 1) *Masked NeRF*: No inpainting; training is performed only on known pixels. 2) *SD Image Cond*: Each image is individually inpainted using SD and then directly used for training. The dataset we use was introduced by NeRFfiller, which occludes the center of each image with a 256×256 region to inpaint (see Figure 5 top). All four methods are trained using 180 equally spaced images and evaluate metrics on the remaining 20 images.

4.2. Further Analysis

The comparison results with Instant3dit are presented in Table 1, where it is evident that VACE14B with LoRA fine-tuning achieves the best overall performance. The grid image inpainting results shown in Figure 6 further support this conclusion. In comparison with NeRFfiller, our method shows a substantial performance advantage, as presented in Table X. This significant lead is well justified, given the quality of our inpainting visual results shown in Figure 1 and Figure 5.

| | FID ↓ | LPIPS ↓ | Clip ↑ |
|--------------------------|-------|---------|--------|
| GT | — | 0.140 | 30.53 |
| Instant3dit (CVPR’25) | 100.9 | 0.253 | 29.81 |
| ObjFiller-3D-1.3B (ours) | 92.07 | 0.190 | 29.87 |
| ObjFiller-3D-14B (ours) | 90.75 | 0.195 | 30.19 |

Table 1. **Quantitative result compare to Instant3dit.** We compare our result with the latest method Instant3dit on three aspect. FID scores are computed between the synthesized images and the ground truth (GT).

Number of Input Views. More incomplete views provide extra object information, but also impose greater constraints. As shown in Table 3, the performance of our inpainter improves with more inputs. Therefore, we argue that our method effectively handles the negative aspects in-

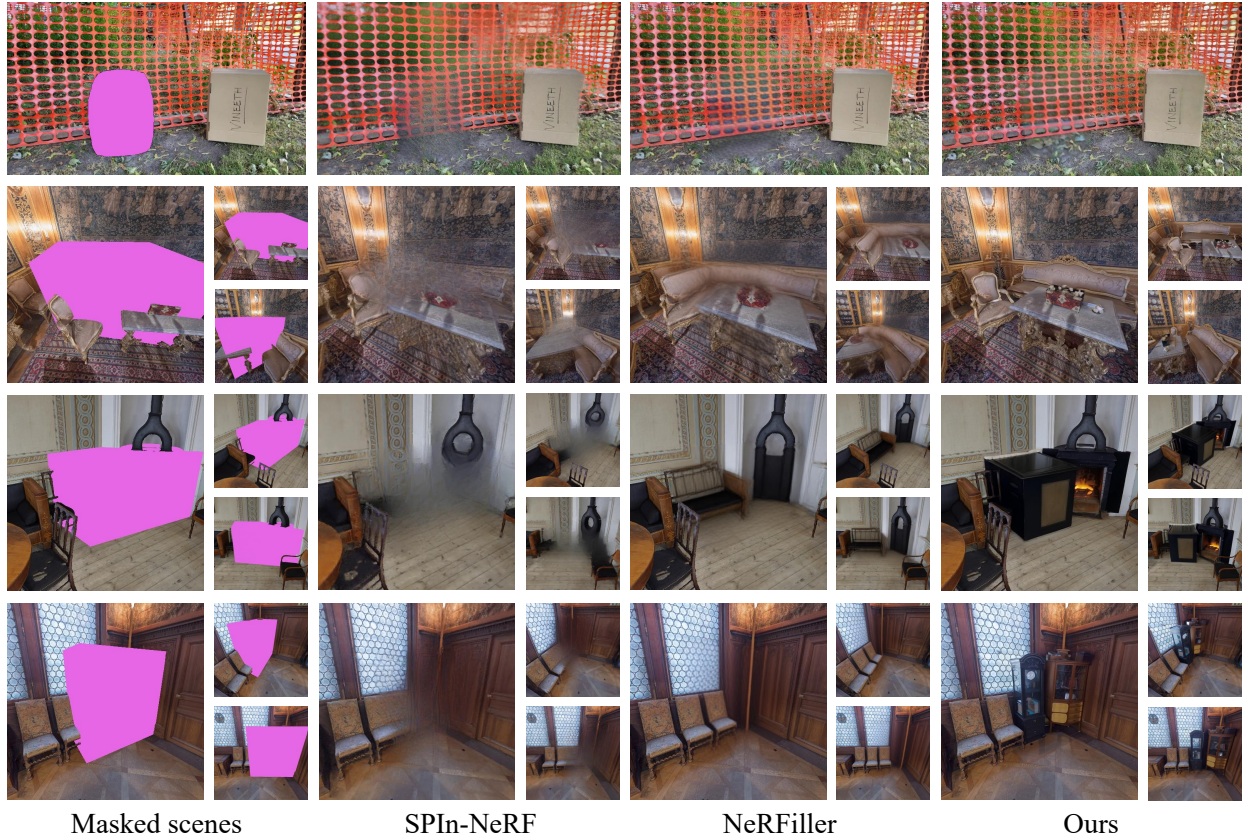


Figure 7. **Qualitative results of scene inpainting.** The leftmost column shows the scenes we need to process, where the areas to be repaired are masked in pink. We compare our method, ObjFiller-3D (the rightmost column), with other approaches.

| | PSNR \uparrow | SSIM \uparrow | LPIPS \downarrow |
|---------------------|-----------------|-----------------|--------------------|
| Masked NeRF | 7.76 | 0.71 | 0.37 |
| SD Image Cond | 14.15 | 0.76 | 0.28 |
| NeRFiller (CVPR'24) | 15.89 | 0.82 | 0.23 |
| Ours | 26.62 | 0.93 | 0.07 |

Table 2. **Quantitative result compare to NeRFiller.** All evaluation metrics have improved by a large margin compared to baselines.

roduced by additional views, while also benefiting from the positive information they provide.

LoRA ablation. A key component of our method is the LoRA weights, which are fine-tuned using three types of multiview-consistent masks. To assess their effectiveness, we conduct ablation studies focusing on this aspect. Figure 8 shows the difference. The quantitative comparisons are provided in the supplementary material.

Extend to 3D Scene. Leveraging our video-based approach, we naturally extend it to 3D scene inpainting,

| Input Views | 80 | 100 | 120 | 140 |
|--------------------|-------|-------|-------|-------|
| PSNR \uparrow | 22.76 | 25.63 | 26.62 | 26.68 |
| SSIM \uparrow | 0.89 | 0.92 | 0.93 | 0.93 |
| LPIPS \downarrow | 0.11 | 0.08 | 0.07 | 0.06 |

Table 3. Evaluation of our 3D inpainting method across different input view number.

which—like object-level inpainting—is fundamentally a mask-filling task. We evaluate our method on four diverse scenes, comparing it with NeRFiller and SPIn-NeRF [30], as shown in Figure 7. Unlike SPIn-NeRF, which assumes compact mask regions suited for object removal, our approach accommodates broader, unconstrained masks, enabling more general 3D inpainting and demonstrating greater applicability. In complex scenes, our method outperforms NeRFiller, as illustrated in the second row of Figure 7.

Applications. Since inpainting and editing are closely related tasks, our model can also be applied to the process of



Figure 8. **LoRA ablation.** We evaluate both w./w.o. LoRA configurations across different parameter scales. As expected, the 14B variant with LoRA delivers the best performance (bottom-left).

object editing. Specifically, we can import our object into Blender, manually place a 3D geometric shape as the 3D mask in the desired location. Figure 9 illustrates an **replace** example. Similarly, ObjFiller-3D supports **add** and **remove**.

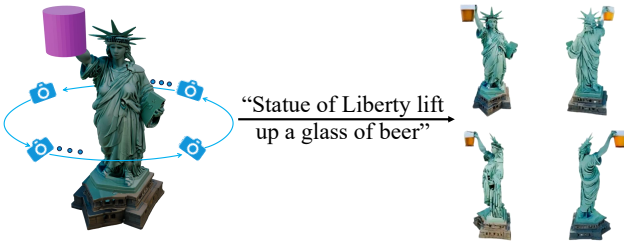


Figure 9. **Object editing.** Given a text prompt, ObjFiller-3D can **replace** the corresponding part of the object accordingly.

5. Conclusion

In this paper, we propose ObjFiller-3D, a fast and consistent 3D inpainting framework adapted an off-the-shelf video diffusion model [18]. By bridging the gap between video and 3D data and introducing reference-guided inpainting, our method overcomes limitations of prior approaches that rely on inconsistent view synthesis or restricted viewpoint priors, achieving high-quality object reconstruction and surpasses prior approaches in fidelity, consistency, and speed. Furthermore, our framework generalizes to 3D scene-level inpainting and object editing, paving the way for broader applications in digital content creation, gaming, cultural heritage restoration, and virtual environments.

Limitation. Our approach is built upon video foundation models, and thus its capabilities are inherently constrained by the limitations of these models. We believe that with the emergence of more powerful video models in the future, the effectiveness of our method will be further enhanced.

Acknowledgement

The computational resources are supported by SongShan Lake HPC Center (SSL-HPC) in Great Bay University. This work was also supported by Guangdong Research Team for Communication and Sensing Integrated with Intelligent Computing (Project No. 2024KCXTD047).

References

- [1] Josh Achiam, Steven Adler, Sandhini Agarwal, Lama Ahmad, Ilge Akkaya, Florencia Leoni Aleman, Diogo Almeida, Janko Altenschmidt, Sam Altman, Shyamal Anadkat, et al. Gpt-4 technical report. *arXiv preprint arXiv:2303.08774*, 2023. 4
- [2] Amir Barda, Matheus Gadelha, Vladimir G Kim, Noam Aigerman, Amit H Bermano, and Thibault Groueix. Instant3dit: Multiview inpainting for fast editing of 3d objects. In *Proceedings of the Computer Vision and Pattern Recognition Conference*, pages 16273–16282, 2025. 2, 3, 1
- [3] Guibin Chen, Dixuan Lin, Jiangping Yang, Chunze Lin, Junchen Zhu, Mingyuan Fan, Hao Zhang, Sheng Chen, Zheng Chen, Chengcheng Ma, et al. Skyreels-v2: Infinite-length film generative model. *arXiv preprint arXiv:2504.13074*, 2025. 3
- [4] Jun-Kun Chen and Yu-Xiong Wang. Proedit: Simple progression is all you need for high-quality 3d scene editing. *Advances in Neural Information Processing Systems*, 37:4934–4955, 2024. 3
- [5] Yiwen Chen, Zilong Chen, Chi Zhang, Feng Wang, Xiaofeng Yang, Yikai Wang, Zhongang Cai, Lei Yang, Huaping Liu, and Guosheng Lin. Gaussianeditor: Swift and controllable 3d editing with gaussian splatting. In *Proceedings of the IEEE/CVF conference on computer vision and pattern recognition*, pages 21476–21485, 2024. 3
- [6] Matt Deitke, Dustin Schwenk, Jordi Salvador, Luca Weihs, Oscar Michel, Eli VanderBilt, Ludwig Schmidt, Kiana Ehsani, Aniruddha Kembhavi, and Ali Farhadi. Objaverse: A universe of annotated 3d objects. In *Proceedings of the IEEE/CVF conference on computer vision and pattern recognition*, pages 13142–13153, 2023. 3, 4
- [7] Chen Gao, Ayush Saraf, Jia-Bin Huang, and Johannes Kopf. Flow-edge guided video completion. In *European Conference on Computer Vision*, pages 713–729. Springer, 2020. 3
- [8] Ruiqi Gao, Aleksander Holynski, Philipp Henzler, Arthur Brussee, Ricardo Martin-Brualla, Pratul Srinivasan, Jonathan T Barron, and Ben Poole. Cat3d: Create anything in 3d with multi-view diffusion models. *arXiv preprint arXiv:2405.10314*, 2024. 3
- [9] David Ha and Jürgen Schmidhuber. World models. *arXiv preprint arXiv:1803.10122*, 2(3), 2018. 2
- [10] Ayaan Haque, Matthew Tancik, Alexei A Efros, Aleksander Holynski, and Angjoo Kanazawa. Instruct-nerf2nerf: Editing 3d scenes with instructions. In *Proceedings of the IEEE/CVF international conference on computer vision*, pages 19740–19750, 2023. 2, 3

- [11] Martin Heusel, Hubert Ramsauer, Thomas Unterthiner, Bernhard Nessler, and Sepp Hochreiter. Gans trained by a two time-scale update rule converge to a local nash equilibrium. *Neural Information Processing Systems, Neural Information Processing Systems*, 2017. 6
- [12] Jonathan Ho and Tim Salimans. Classifier-free diffusion guidance. *arXiv preprint arXiv:2207.12598*, 2022. 6
- [13] Jonathan Ho, William Chan, Chitwan Saharia, Jay Whang, Ruiqi Gao, Alexey Gritsenko, Diederik P Kingma, Ben Poole, Mohammad Norouzi, David J Fleet, et al. Imagen video: High definition video generation with diffusion models. *arXiv preprint arXiv:2210.02303*, 2022. 2
- [14] Yicong Hong, Kai Zhang, Jiuxiang Gu, Sai Bi, Yang Zhou, Difan Liu, Feng Liu, Kalyan Sunkavalli, Trung Bui, and Hao Tan. Lrm: Large reconstruction model for single image to 3d. *arXiv preprint arXiv:2311.04400*, 2023. 2, 3
- [15] Edward J Hu, Yelong Shen, Phillip Wallis, Zeyuan Allen-Zhu, Yuanzhi Li, Shean Wang, Lu Wang, Weizhu Chen, et al. Lora: Low-rank adaptation of large language models. *ICLR*, 1(2):3, 2022. 2, 5
- [16] Yukun Huang, Jianan Wang, Yukai Shi, Xianbiao Qi, Zheng-Jun Zha, and Lei Zhang. Dreamtime: An improved optimization strategy for text-to-3d content creation. *arXiv preprint arXiv:2306.12422*, 3(5):14, 2023. 3
- [17] Zehuan Huang, Yuan-Chen Guo, Haoran Wang, Ran Yi, Lizhuang Ma, Yan-Pei Cao, and Lu Sheng. Mv-adapter: Multi-view consistent image generation made easy. *arXiv preprint arXiv:2412.03632*, 2024. 3
- [18] Zeyinzi Jiang, Zhen Han, Chaojie Mao, Jingfeng Zhang, Yulin Pan, and Yu Liu. Vace: All-in-one video creation and editing. *arXiv preprint arXiv:2503.07598*, 2025. 2, 3, 4, 8
- [19] James T Kajiya and Brian P Von Herzen. Ray tracing volume densities. *ACM SIGGRAPH computer graphics*, 18(3):165–174, 1984. 3
- [20] Bernhard Kerbl, Georgios Kopanas, Thomas Leimkühler, and George Drettakis. 3d gaussian splatting for real-time radiance field rendering. *ACM Trans. Graph.*, 42(4):139–1, 2023. 3
- [21] Weijie Kong, Qi Tian, Zijian Zhang, Rox Min, Zuozhuo Dai, Jin Zhou, Jiangfeng Xiong, Xin Li, Bo Wu, Jianwei Zhang, et al. Hunyuanvideo: A systematic framework for large video generative models. *arXiv preprint arXiv:2412.03603*, 2024. 3
- [22] Junnan Li, Dongxu Li, Silvio Savarese, and Steven Hoi. Blip-2: Bootstrapping language-image pre-training with frozen image encoders and large language models. In *International conference on machine learning*, pages 19730–19742. PMLR, 2023. 4
- [23] Jiahao Li, Hao Tan, Kai Zhang, Zexiang Xu, Fujun Luan, Yinghao Xu, Yicong Hong, Kalyan Sunkavalli, Greg Shakhnarovich, and Sai Bi. Instant3d: Fast text-to-3d with sparse-view generation and large reconstruction model. *arXiv preprint arXiv:2311.06214*, 2023. 2, 3, 1
- [24] Yuan Liu, Cheng Lin, Zijiao Zeng, Xiaoxiao Long, Lingjie Liu, Taku Komura, and Wenping Wang. Syncdreamer: Generating multiview-consistent images from a single-view image. *arXiv preprint arXiv:2309.03453*, 2023. 3
- [25] Zhiheng Liu, Hao Ouyang, Qiuyu Wang, Ka Leong Cheng, Jie Xiao, Kai Zhu, Nan Xue, Yu Liu, Yujun Shen, and Yang Cao. Infusion: Inpainting 3d gaussians via learning depth completion from diffusion prior. *arXiv preprint arXiv:2404.11613*, 2024. 3
- [26] Xiaoxiao Long, Yuan-Chen Guo, Cheng Lin, Yuan Liu, Zhiyang Dou, Lingjie Liu, Yuexin Ma, Song-Hai Zhang, Marc Habermann, Christian Theobalt, et al. Wonder3d: Single image to 3d using cross-domain diffusion. In *Proceedings of the IEEE/CVF conference on computer vision and pattern recognition*, pages 9970–9980, 2024. 3
- [27] Andreas Lugmayr, Martin Danelljan, Andres Romero, Fisher Yu, Radu Timofte, and Luc Van Gool. Repaint: Inpainting using denoising diffusion probabilistic models. In *Proceedings of the IEEE/CVF conference on computer vision and pattern recognition*, pages 11461–11471, 2022. 2
- [28] Tiange Luo, Chris Rockwell, Honglak Lee, and Justin Johnson. Scalable 3d captioning with pretrained models. *Advances in Neural Information Processing Systems*, 36: 75307–75337, 2023. 4, 6
- [29] Ben Mildenhall, Pratul P Srinivasan, Matthew Tancik, Jonathan T Barron, Ravi Ramamoorthi, and Ren Ng. Nerf: Representing scenes as neural radiance fields for view synthesis. *Communications of the ACM*, 65(1):99–106, 2021. 3
- [30] Ashkan Mirzaei, Tristan Aumentado-Armstrong, Konstantinos G Derpanis, Jonathan Kelly, Marcus A Brubaker, Igor Gilitschenski, and Alex Levinstein. Spin-nerf: Multiview segmentation and perceptual inpainting with neural radiance fields. In *Proceedings of the IEEE/CVF Conference on Computer Vision and Pattern Recognition*, pages 20669–20679, 2023. 3, 7
- [31] Dustin Podell, Zion English, Kyle Lacey, Andreas Blattmann, Tim Dockhorn, Jonas Müller, Joe Penna, and Robin Rombach. Sdxl: Improving latent diffusion models for high-resolution image synthesis. *arXiv preprint arXiv:2307.01952*, 2023. 6
- [32] Ben Poole, Ajay Jain, Jonathan T Barron, and Ben Mildenhall. Dreamfusion: Text-to-3d using 2d diffusion. *arXiv preprint arXiv:2209.14988*, 2022. 2, 3
- [33] Alec Radford, Jong Wook Kim, Chris Hallacy, Aditya Ramesh, Gabriel Goh, Sandhini Agarwal, Girish Sastry, Amanda Askell, Pamela Mishkin, Jack Clark, et al. Learning transferable visual models from natural language supervision. In *International conference on machine learning*, pages 8748–8763. PmLR, 2021. 4, 6
- [34] Robin Rombach, Andreas Blattmann, Dominik Lorenz, Patrick Esser, and Björn Ommer. High-resolution image synthesis with latent diffusion models. In *Proceedings of the IEEE/CVF conference on computer vision and pattern recognition*, pages 10684–10695, 2022. 3
- [35] Chitwan Saharia, William Chan, Saurabh Saxena, Lala Li, Jay Whang, Emily L Denton, Kamyar Ghasemipour, Raphael Gontijo Lopes, Burcu Karagol Ayan, Tim Salimans, et al. Photorealistic text-to-image diffusion models with deep language understanding. *Advances in neural information processing systems*, 35:36479–36494, 2022. 3

- [36] Christoph Schuhmann, Richard Vencu, Romain Beaumont, Robert Kaczmarczyk, Clayton Mullis, Aarush Katta, Theo Coombes, Jenia Jitsev, and Aran Komatsuzaki. Laion-400m: Open dataset of clip-filtered 400 million image-text pairs. *arXiv preprint arXiv:2111.02114*, 2021. 3
- [37] Christoph Schuhmann, Romain Beaumont, Richard Vencu, Cade Gordon, Ross Wightman, Mehdi Cherti, Theo Coombes, Aarush Katta, Clayton Mullis, Mitchell Wortsman, et al. Laion-5b: An open large-scale dataset for training next generation image-text models. *Advances in neural information processing systems*, 35:25278–25294, 2022. 3
- [38] Ruoxi Shi, Hansheng Chen, Zhuoyang Zhang, Minghua Liu, Chao Xu, Xinyue Wei, Linghao Chen, Chong Zeng, and Hao Su. Zero123++: a single image to consistent multi-view diffusion base model. *arXiv preprint arXiv:2310.15110*, 2023. 3
- [39] Yichun Shi, Peng Wang, Jianglong Ye, Mai Long, Kejie Li, and Xiao Yang. Mvdream: Multi-view diffusion for 3d generation. *arXiv preprint arXiv:2308.16512*, 2023. 3
- [40] Zhihao Shi, Dong Huo, Yuhongze Zhou, Yan Min, Juwei Lu, and Xinxin Zuo. Imfine: 3d inpainting via geometry-guided multi-view refinement. In *Proceedings of the Computer Vision and Pattern Recognition Conference*, pages 26694–26703, 2025. 3
- [41] Roman Suvorov, Elizaveta Logacheva, Anton Mashikhin, Anastasia Remizova, Arsenii Ashukha, Aleksei Silvestrov, Naejin Kong, Harshith Goka, Kiwoong Park, and Victor Lempitsky. Resolution-robust large mask inpainting with fourier convolutions. In *Proceedings of the IEEE/CVF winter conference on applications of computer vision*, pages 2149–2159, 2022. 2
- [42] Vikram Voleti, Chun-Han Yao, Mark Boss, Adam Letts, David Pankratz, Dmitry Tochilkin, Christian Laforte, Robin Rombach, and Varun Jampani. Sv3d: Novel multi-view synthesis and 3d generation from a single image using latent video diffusion. In *European Conference on Computer Vision*, pages 439–457. Springer, 2024. 2
- [43] Team Wan, Ang Wang, Baole Ai, Bin Wen, Chaojie Mao, Chen-Wei Xie, Di Chen, Feiwei Yu, Haiming Zhao, Jianxiao Yang, et al. Wan: Open and advanced large-scale video generative models. *arXiv preprint arXiv:2503.20314*, 2025. 2, 3
- [44] Peng Wang and Yichun Shi. Imagedream: Image-prompt multi-view diffusion for 3d generation. *arXiv preprint arXiv:2312.02201*, 2023. 3
- [45] Wen Wang, Yan Jiang, Kangyang Xie, Zide Liu, Hao Chen, Yue Cao, Xinlong Wang, and Chunhua Shen. Zero-shot video editing using off-the-shelf image diffusion models. *arXiv preprint arXiv:2303.17599*, 2023. 2
- [46] Wenjing Wang, Huan Yang, Zixi Tuo, Huiguo He, Junchen Zhu, Jianlong Fu, and Jiaying Liu. Videofactory: Swap attention in spatiotemporal diffusions for text-to-video generation. *arXiv preprint arXiv:2305.10874*, 2023. 3
- [47] Yuxuan Wang, Xuanyu Yi, Zike Wu, Na Zhao, Long Chen, and Hanwang Zhang. View-consistent 3d editing with gaussian splatting. In *European conference on computer vision*, pages 404–420. Springer, 2024. 3
- [48] Zhengyi Wang, Cheng Lu, Yikai Wang, Fan Bao, Chongxuan Li, Hang Su, and Jun Zhu. Prolificdreamer: High-fidelity and diverse text-to-3d generation with variational score distillation. *Advances in neural information processing systems*, 36: 8406–8441, 2023. 3
- [49] Ethan Weber, Aleksander Holynski, Varun Jampani, Saurabh Saxena, Noah Snively, Abhishek Kar, and Angjoo Kanazawa. Nerfiller: Completing scenes via generative 3d inpainting. In *Proceedings of the IEEE/CVF Conference on Computer Vision and Pattern Recognition*, pages 20731–20741, 2024. 2, 3, 5, 1
- [50] Xinyue Wei, Kai Zhang, Sai Bi, Hao Tan, Fujun Luan, Valentin Deschaintre, Kalyan Sunkavalli, Hao Su, and Zexiang Xu. Meshlrn: Large reconstruction model for high-quality meshes. *arXiv preprint arXiv:2404.12385*, 2024. 3
- [51] Chung-Ho Wu, Yang-Jung Chen, Ying-Huan Chen, Jie-Ying Lee, Bo-Hsu Ke, Chun-Wei Tuan Mu, Yi-Chuan Huang, Chin-Yang Lin, Min-Hung Chen, Yen-Yu Lin, et al. Aurafusion360: Augmented unseen region alignment for reference-based 360deg unbounded scene inpainting. In *Proceedings of the Computer Vision and Pattern Recognition Conference*, pages 16366–16376, 2025. 3
- [52] Jianfeng Xiang, Zelong Lv, Sicheng Xu, Yu Deng, Ruicheng Wang, Bowen Zhang, Dong Chen, Xin Tong, and Jiaolong Yang. Structured 3d latents for scalable and versatile 3d generation. In *Proceedings of the Computer Vision and Pattern Recognition Conference*, pages 21469–21480, 2025. 2
- [53] Jiale Xu, Weihao Cheng, Yiming Gao, Xintao Wang, Shenghua Gao, and Ying Shan. Instantmesh: Efficient 3d mesh generation from a single image with sparse-view large reconstruction models. *arXiv preprint arXiv:2404.07191*, 2024. 3, 6, 1
- [54] Rui Xu, Xiaoxiao Li, Bolei Zhou, and Chen Change Loy. Deep flow-guided video inpainting. In *Proceedings of the IEEE/CVF conference on computer vision and pattern recognition*, pages 3723–3732, 2019. 3
- [55] Hongwei Xue, Tiankai Hang, Yanhong Zeng, Yuchong Sun, Bei Liu, Huan Yang, Jianlong Fu, and Baining Guo. Advancing high-resolution video-language representation with large-scale video transcriptions. In *International Conference on Computer Vision and Pattern Recognition (CVPR)*, 2022. 3
- [56] Wilson Yan, Yunzhi Zhang, Pieter Abbeel, and Aravind Srinivas. Videogpt: Video generation using vq-vae and transformers. *arXiv preprint arXiv:2104.10157*, 2021. 2
- [57] Richard Zhang, Phillip Isola, Alexei A. Efros, Eli Shechtman, and Oliver Wang. The unreasonable effectiveness of deep features as a perceptual metric. In *2018 IEEE/CVF Conference on Computer Vision and Pattern Recognition*, 2018. 6
- [58] Wenliang Zhao, Lujia Bai, Yongming Rao, Jie Zhou, and Jiwen Lu. Unipc: A unified predictor-corrector framework for fast sampling of diffusion models. *Advances in Neural Information Processing Systems*, 36:49842–49869, 2023. 5
- [59] Shangchen Zhou, Chongyi Li, Kelvin CK Chan, and Chen Change Loy. Propainter: Improving propagation and transformer for video inpainting. In *Proceedings of*

the IEEE/CVF international conference on computer vision,
pages 10477–10486, 2023. [3](#)

ObjFiller-3D: Consistent Multi-view 3D Inpainting via Video Diffusion Models

Supplementary Material

I. Dataset Details

Rendering Setup. We generate perspectives of each object against a plain white background under uniform lighting conditions using Blender’s physically-based path tracer Cycles. Before rendering, the selected 3D models are uniformly resized and aligned at the center of a bounded cubic space defined by $[-1, 1]^3$. The entire setup conforms to a systematic configuration (see Data Preparation section of the main text.), employing a fov of 50° from a fixed range of 2.7 units to produce 16 distinct renderings.

All rendered images and associated metadata used in our experiments will be made publicly available upon publication. We believe this will serve as a valuable inspiration for future work.

Prompts Used for Dataset. We use the following text prompts for each of the 8 NeRF synthetic object and 4 scenes from NeRFiller [49].

- “chair”: “A video of a green striped chair.”
- “drums”: “A video of drums.”
- “fics”: “A video of fics.”
- “hotdog”: “A video of golden brown hotdogs with mustard and condiments.”
- “lego”: “A video of LEGO bulldozer model.”
- “materials”: “A video of 3D models displaying diverse material textures and finishes.”
- “mic”: “A video of a microphone.”
- “ship”: “A video of a ship in a circular basin.”
- “backpack”: “A black backpack and a cardboard box rest on the grass in front of an orange plastic fence.”
- “billiards”: “A video of a vintage-style room.”
- “drawing”: “A video of a lavish interior.”
- “norway”: “A video of an elegant room.”

II. More Experimental Implementation

Evaluation Metrics. To compare perceptual similarity between our method and Instant3dit [2], we adopt the LPIPS metric using VGG as the backbone network. Since the original reconstruction module (LRM: Instant3D [23]) used in Instant3dit is not publicly available, we employ InstantMesh [53] as a unified reconstruction backend to ensure a fair comparison. InstantMesh reconstructs 3D meshes from four orthographic-view input images and renders synthesized views using a triplane-based rendering module and the associated camera parameters. These rendered images are then used for the LPIPS evaluation. For CLIP-based comparisons, we use

the pretrained weights CLIP-ViT-L-14-CommonPool.XL-s13B-b90K¹ from the Hugging Face Hub. CLIP metrics assess semantic consistency between the rendered results and the reference inputs, providing a complementary evaluation to LPIPS.

Training Setup During our fine-tuning process, the VACE1.3B model was trained using full-precision on an NVIDIA RTX 4090 GPU, with an approximate memory usage of 20 GB. In contrast, the VACE14B model was trained using half-precision on an NVIDIA A800 GPU, requiring approximately 60 GB of memory. Both models were trained for 10 epochs, with each epoch comprising 3,000 steps. The training of a single epoch typically required around 6 hours, depending on hardware conditions and model size.

| | FID ↓ | LPIPS ↓ | Clip ↑ |
|-----------------|-------|---------|--------|
| w/o LoRA (1.3B) | 107.2 | 0.205 | 29.76 |
| w/ LoRA (1.3B) | 92.07 | 0.190 | 29.87 |

Table I. Quantitative result of LoRA ablation on the 1.3B model.

| | FID ↓ | LPIPS ↓ | Clip ↑ |
|----------------|-------|---------|--------|
| w/o LoRA (14B) | 104.8 | 0.219 | 30.19 |
| w/ LoRA (14B) | 90.75 | 0.195 | 30.19 |

Table II. Quantitative result of LoRA ablation on the 14B model.

III. Additional Results

Figure I presents additional visualization results for comparative analysis with Instant3dit. Table I and Table II show the quantitative comparisons of LoRA ablation. Tables III to X present the individual results for each of the eight objects in the NeRFiller dataset.

¹<https://huggingface.co/laion/CLIP-ViT-L-14-CommonPool.XL-s13B-b90K>

| | PSNR \uparrow | SSIM \uparrow | LPIPS \downarrow |
|---------------------|-----------------|-----------------|--------------------|
| Masked NeRF | 5.19 | 0.70 | 0.40 |
| SD Image Cond | 13.71 | 0.75 | 0.31 |
| NeRFiller (CVPR'24) | 16.59 | 0.85 | 0.24 |
| Ours | 30.74 | 0.96 | 0.03 |

Table III. Quantitative evaluation of inpainting consistency on “chair” data.

| | PSNR \uparrow | SSIM \uparrow | LPIPS \downarrow |
|---------------------|-----------------|-----------------|--------------------|
| Masked NeRF | 5.77 | 0.66 | 0.49 |
| SD Image Cond | 12.30 | 0.76 | 0.27 |
| NeRFiller (CVPR'24) | 13.25 | 0.79 | 0.27 |
| Ours | 21.65 | 0.89 | 0.11 |

Table IV. Quantitative evaluation of inpainting consistency on “drums” data.

| | PSNR \uparrow | SSIM \uparrow | LPIPS \downarrow |
|---------------------|-----------------|-----------------|--------------------|
| Masked NeRF | 6.86 | 0.73 | 0.37 |
| SD Image Cond | 13.40 | 0.76 | 0.31 |
| NeRFiller (CVPR'24) | 17.24 | 0.85 | 0.21 |
| Ours | 26.83 | 0.94 | 0.04 |

Table V. Quantitative evaluation of inpainting consistency on “ficus” data.

| | PSNR \uparrow | SSIM \uparrow | LPIPS \downarrow |
|---------------------|-----------------|-----------------|--------------------|
| Masked NeRF | 8.84 | 0.73 | 0.36 |
| SD Image Cond | 15.12 | 0.78 | 0.31 |
| NeRFiller (CVPR'24) | 16.69 | 0.86 | 0.24 |
| Ours | 29.67 | 0.95 | 0.04 |

Table VI. Quantitative evaluation of inpainting consistency on “hotdog” data.

| | PSNR \uparrow | SSIM \uparrow | LPIPS \downarrow |
|---------------------|-----------------|-----------------|--------------------|
| Masked NeRF | 8.80 | 0.73 | 0.33 |
| SD Image Cond | 14.79 | 0.79 | 0.22 |
| NeRFiller (CVPR'24) | 17.89 | 0.84 | 0.18 |
| Ours | 26.38 | 0.91 | 0.07 |

Table VII. Quantitative evaluation of inpainting consistency on “lego” data.

| | PSNR \uparrow | SSIM \uparrow | LPIPS \downarrow |
|---------------------|-----------------|-----------------|--------------------|
| Masked NeRF | 8.28 | 0.72 | 0.33 |
| SD Image Cond | 14.53 | 0.78 | 0.25 |
| NeRFiller (CVPR'24) | 14.53 | 0.80 | 0.23 |
| Ours | 26.18 | 0.93 | 0.06 |

Table VIII. Quantitative evaluation of inpainting consistency on “materials” data.

| | PSNR \uparrow | SSIM \uparrow | LPIPS \downarrow |
|---------------------|-----------------|-----------------|--------------------|
| Masked NeRF | 6.94 | 0.73 | 0.35 |
| SD Image Cond | 13.40 | 0.77 | 0.28 |
| NeRFiller (CVPR'24) | 13.26 | 0.81 | 0.27 |
| Ours | 25.20 | 0.95 | 0.07 |

Table IX. Quantitative evaluation of inpainting consistency on “mic” data.

| | PSNR \uparrow | SSIM \uparrow | LPIPS \downarrow |
|---------------------|-----------------|-----------------|--------------------|
| Masked NeRF | 10.66 | 0.69 | 0.35 |
| SD Image Cond | 15.95 | 0.74 | 0.29 |
| NeRFiller (CVPR'24) | 17.64 | 0.80 | 0.24 |
| Ours | 26.29 | 0.88 | 0.10 |

Table X. Quantitative evaluation of inpainting consistency on “ship” data.

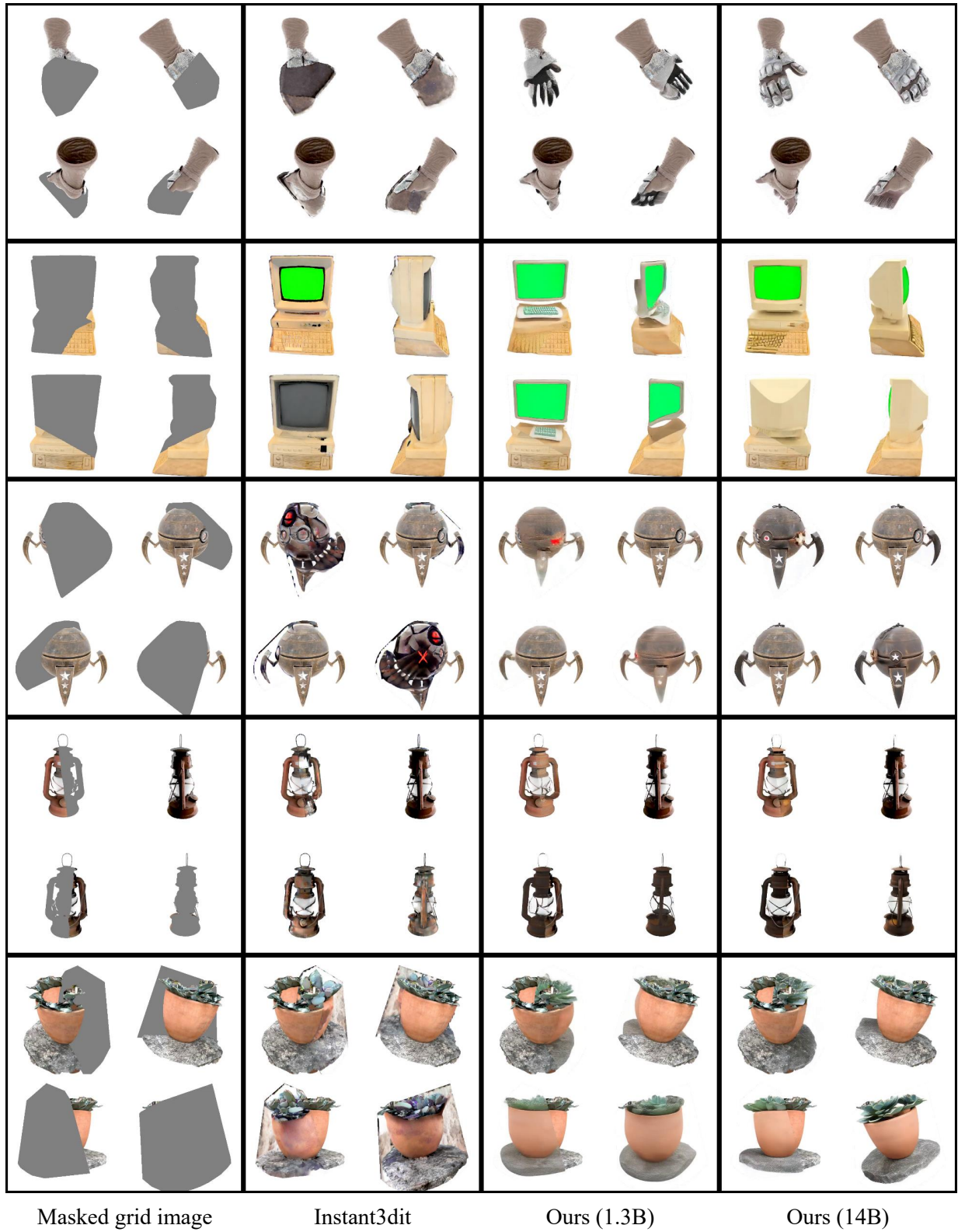


Figure I. **Additional visualization results compared to Instant3dit.** We randomly select several outputs from our method and Instant3dit for qualitative comparison. Overall, our 14B model demonstrates superior consistency across multiple views.